Electronic Supplementary Material (ESI) for Nanoscale.

Constructing tetrahedral CoO_4 vacancies for activating the high oxygen evolution activity of $Co_{3-x}O_{4-\delta}$ porous nanosheet arrays

Shenghua Ye, Yu Zhang, Wei Xiong, Tingting Xu, Peng Liao, Pingyu Zhang, Xiangzhong Ren, Chuanxin He, Lirong Zheng, Xiaoping Ouyang, Qianling Zhang,* and Jianhong Liu,*

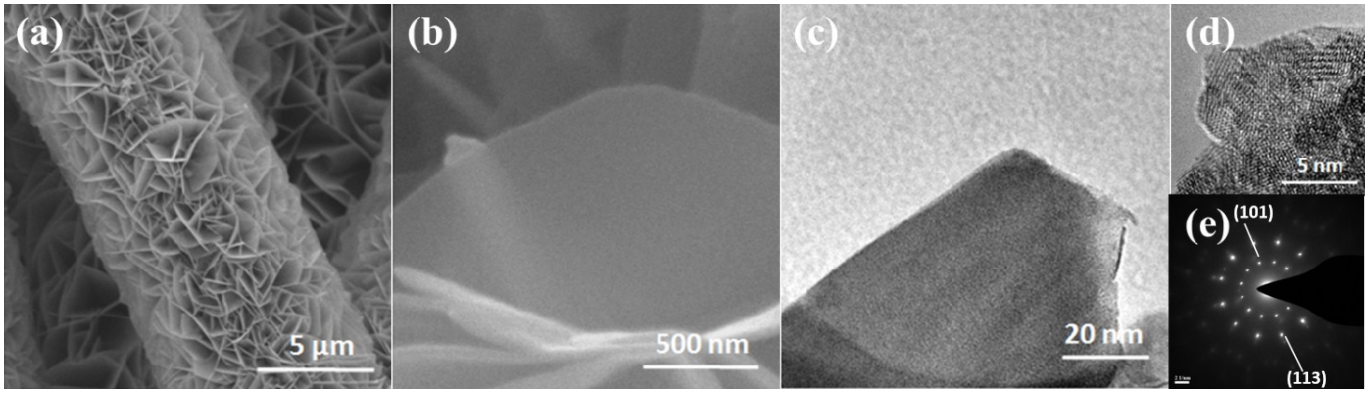

Figure S1 (a–b) SEM, (c) TEM, (d) HRTEM images and (e) SAED pattern of α-$Co(OH)_2$ NAs/CFC.

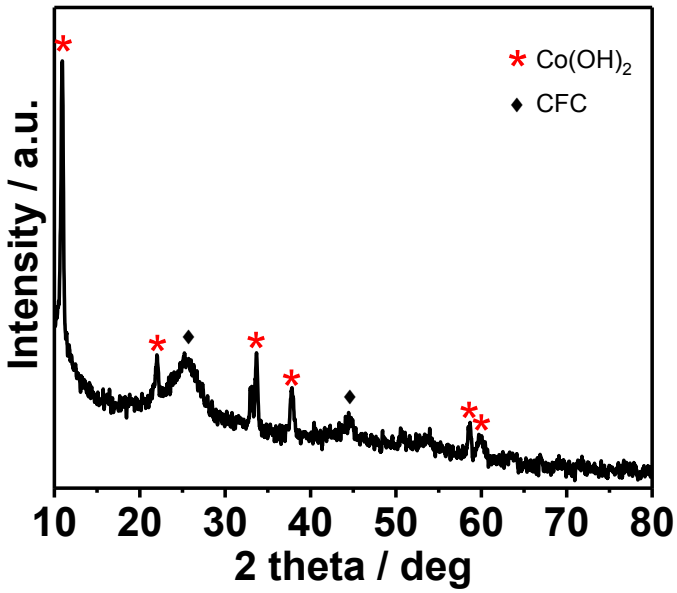

Figure S2 XRD pattern of α-$Co(OH)_2$ NAs/CFC.

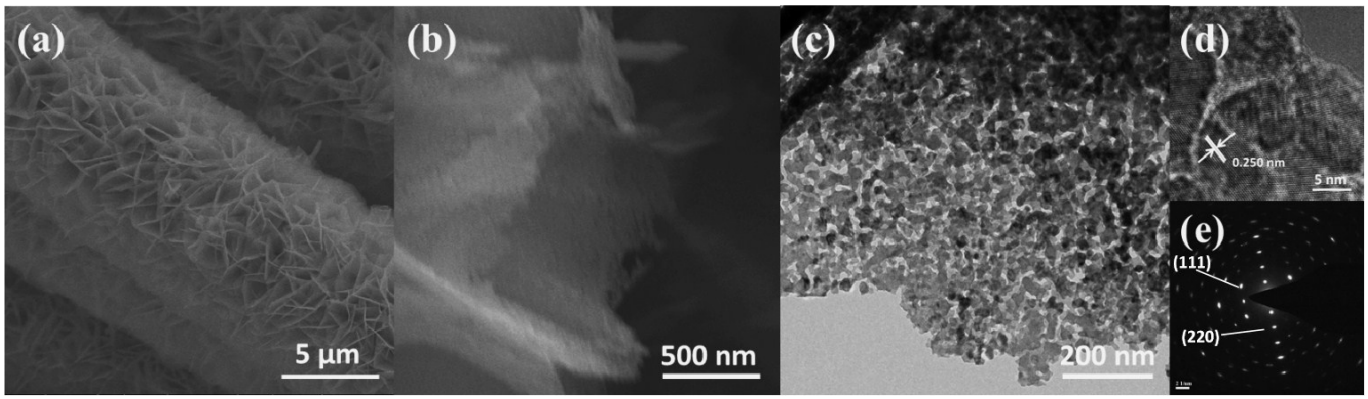

Figure S3 (a–b) SEM, (c) TEM, and (d) HRTEM images, and (e) SAED pattern of CoO PNAs/CFC.

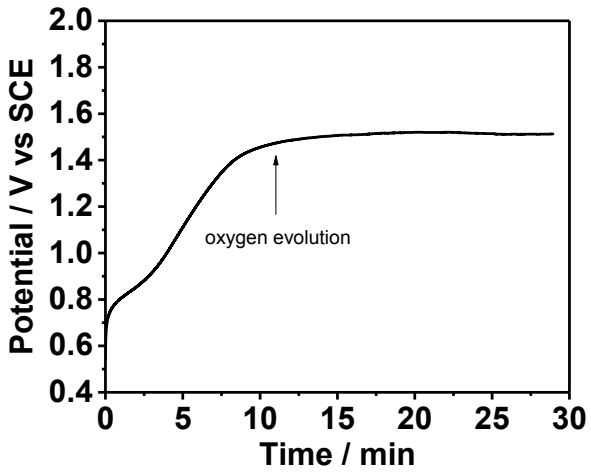

Figure S4 E-t curve during in situ anodic oxidation of CoO PNAs/CFC in a 0.01 M $(NH_4)_2SO_4$ solution.

As shown in Figure S4, the applied potential was lower and increased over time in the first 10 min of the in situ oxidation process. At this stage, CoO gradually transformed to $Co_{3-x}O_{4-\delta}$, and the color of the sample changed from brown to black. After ~10 min, the potential remained stable, and some continuous bubbles appeared, indicating that CoO was thoroughly transformed to $Co_{3-x}O_{4-\delta}$ and the H_2O in the $(NH_4)_2SO_4$ solution began to decompose to O_2 at the anode. To guarantee thoroughly transformed of the sample, we performed the in situ oxidation process for 20 min.

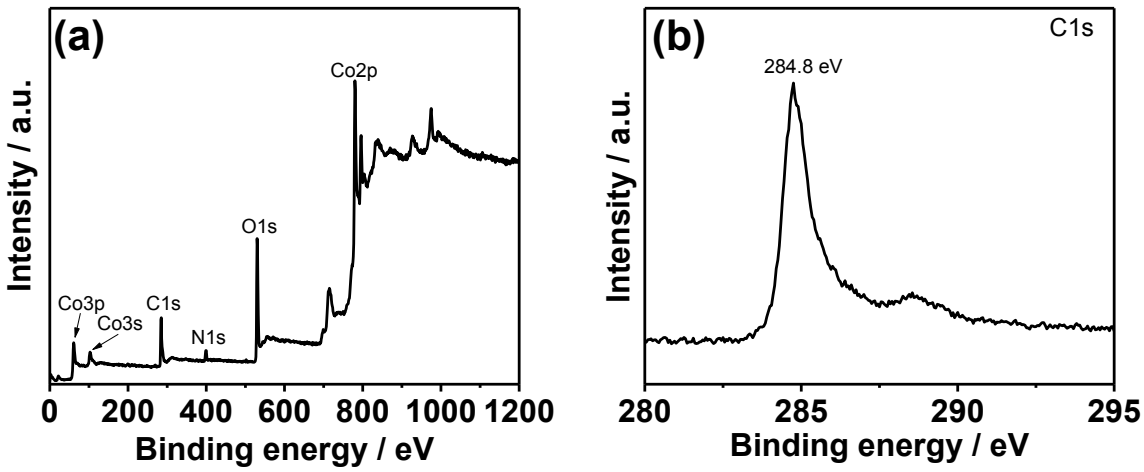

Figure S5 (a) Survey and (b) C1s spectra of $Co_{3-x}O_{4-\delta}$ PNAs/CFC.

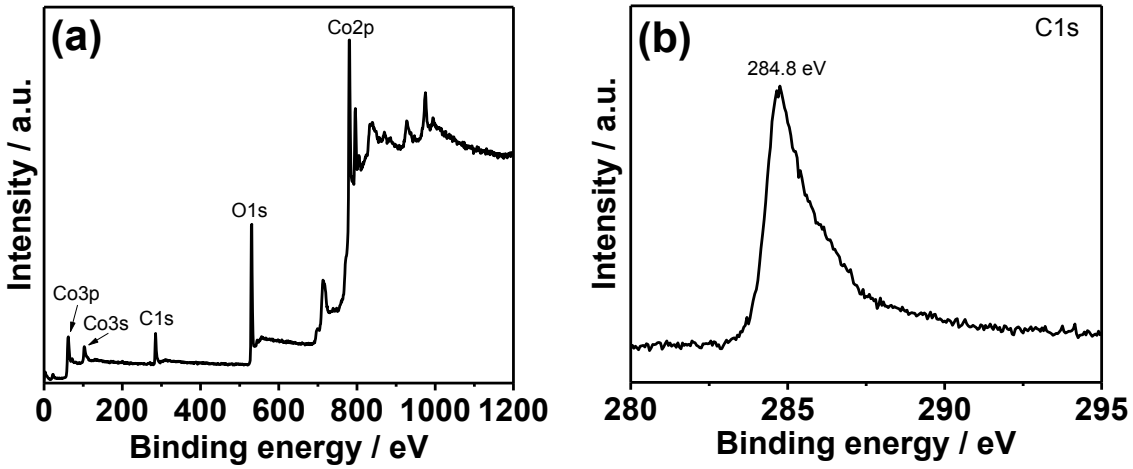

Figure S6 (a) Survey and (b) C1s spectra of Co_3O_4 PNAs/CFC.

The survey spectra of $Co_{3-x}O_{4-\delta}$ PNAs/CFC and Co_3O_4 PNAs/CFC, shown in Figures S5–6, suggest that only C, O, and Co can be detected, along with trace amounts of N that originate from absorbed NH_4^+ on the surface.

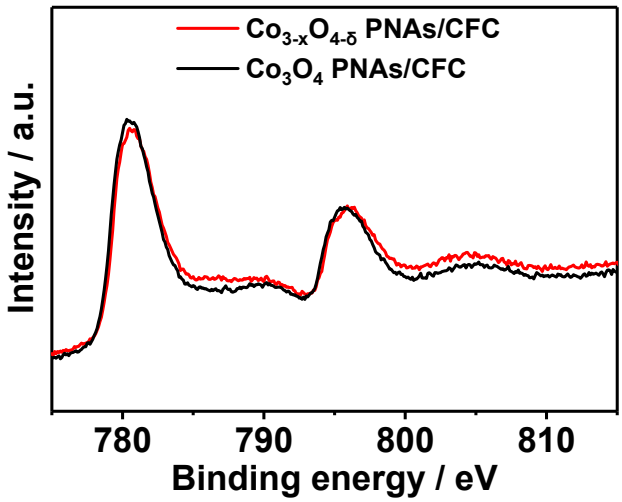

Figure S7 Co2p spectra of $Co_{3-x}O_{4-\delta}$ PNAs/CFC and Co_3O_4 PNAs/CFC.

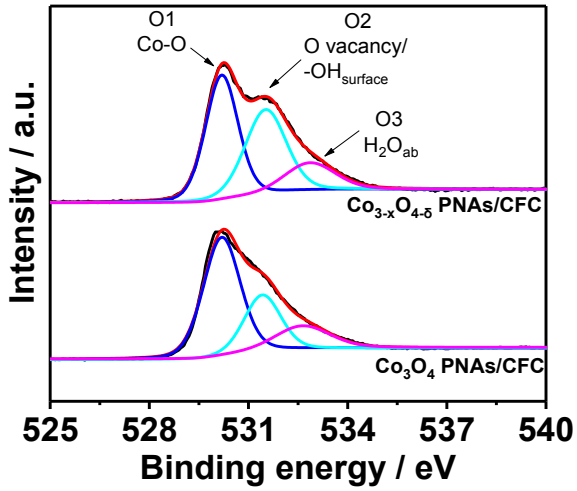

Figure S8 O1s spectra of $Co_{3-x}O_{4-\delta}$ PNAs/CFC and Co_3O_4 PNAs/CFC.

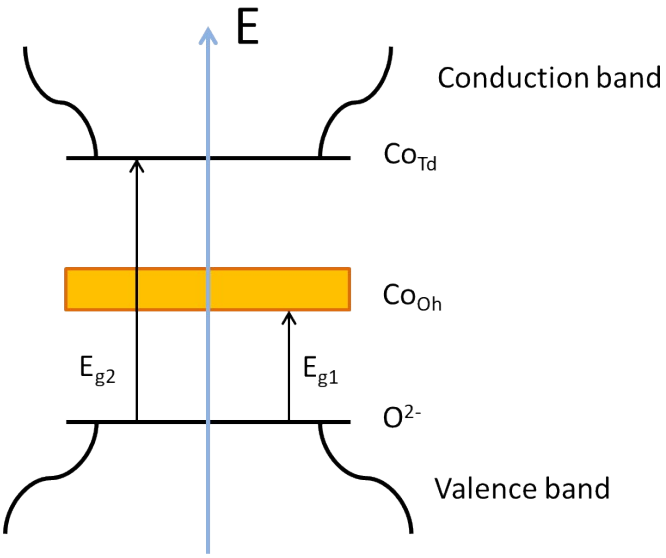

Figure S9 Electronic band structure of Co_3O_4.[1]

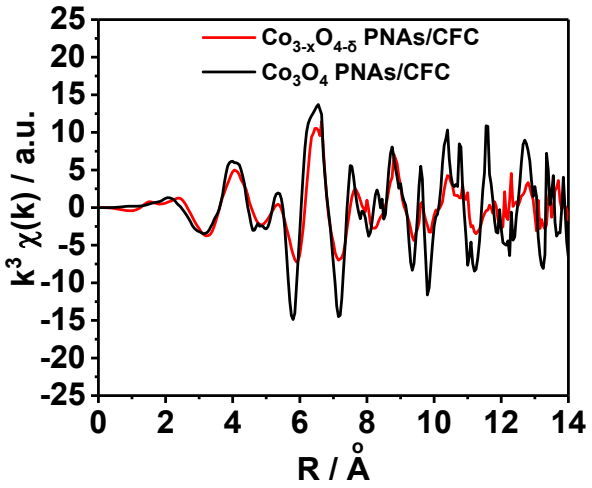

Figure S10 EXAFS oscillation of Co K-edge of $Co_{3-x}O_{4-\delta}$ PNAs/CFC and Co_3O_4 PNAs/CFC.

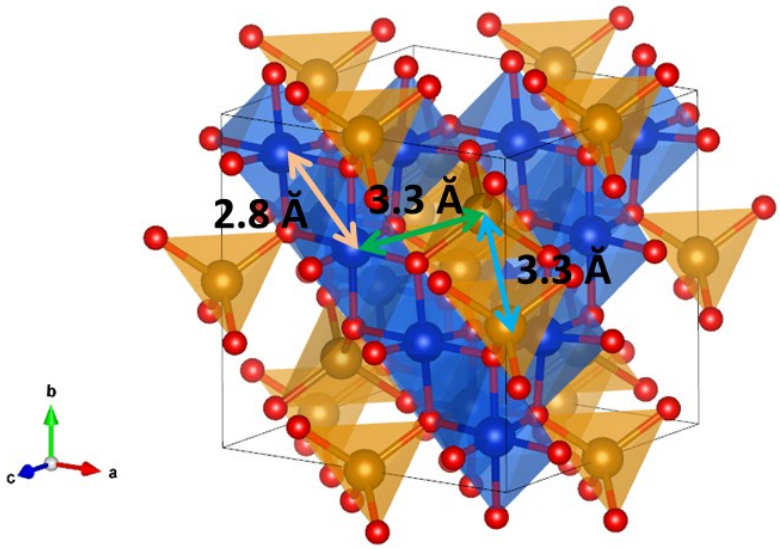

Figure S11 Crystalline structure of Co_3O_4.

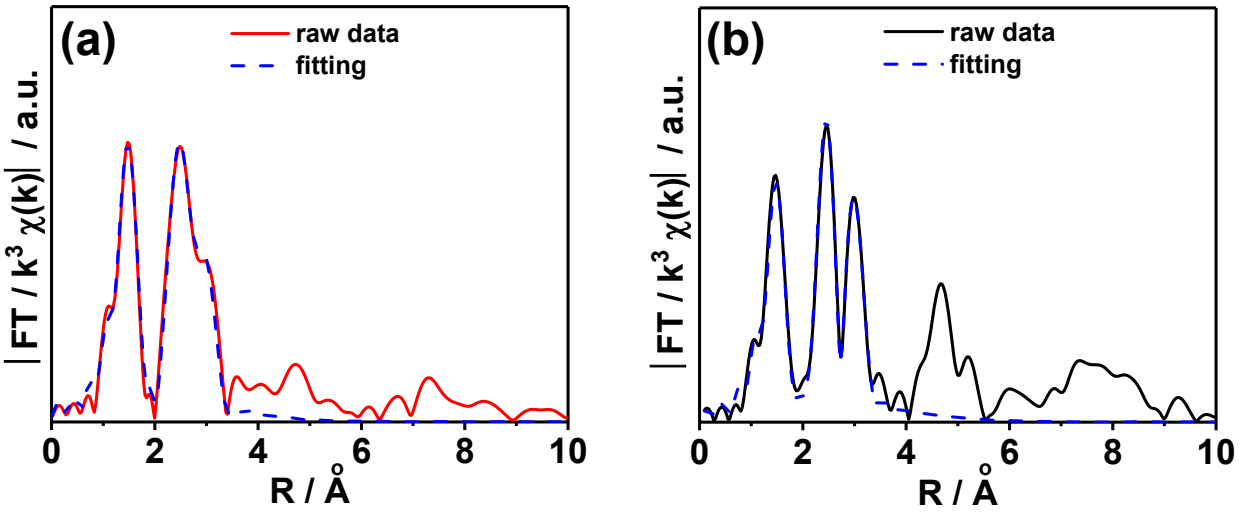

Figure S12 EXAFS fittings of Co K-edge of (a) $Co_{3-x}O_{4-\delta}$ PNAs/CFC and (b) Co_3O_4 PNAs/CFC.

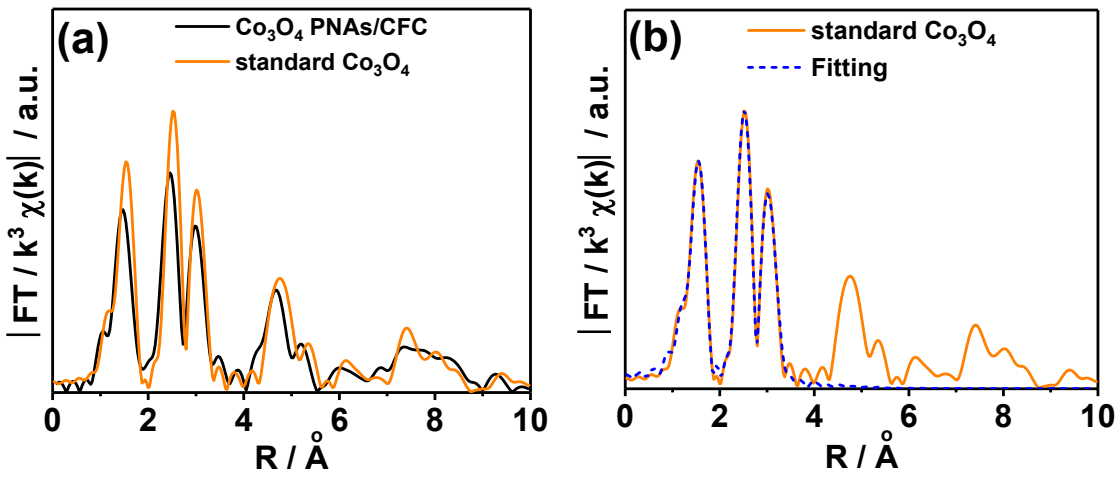

Figure S13 (a) FT-EXAFS of Co K-edge for$Co_{3-x}O_{4-\delta}$ PNAs/CFC and standard Co_3O_4, and (b) EXAFS fitting of standard Co_3O_4.

Table S1. EXAFS fitting parameters of the Co K-edge for various samples.

Sample	Shell	*CN* [a]	*R* (Å) [b]	σ^2 (Å^2·10^3) [c]	ΔE_0 (eV) [d]	*R* factor (%)
$Co_{3-x}O_{4-\delta}$ PNAs/CFC	Co-O	3.9	1.92	4.5	−3.5	1.0
	Co_{Oh}-Co_{Oh}	3.8	2.86	7.8	−4.4	
	Co-Co_{Td}	6.6	3.32	9.3	−8.6	
Co_3O_4 PNAs/CFC	Co-O	5.3	1.92	4.0	−5.6	0.8
	Co_{Oh}-Co_{Oh}	4.0	2.85	3.9	−6.6	
	Co-Co_{Td}	8.1	3.35	6.2	−8.9	
Standard Co_3O_4	Co-O	5.3	1.92	3.3	5.3	0.3
	Co_{Oh}-Co_{Oh}	4.0	2.85	3.4	2.9	
	Co-Co_{Td}	8.0	3.36	7.6		

[a] *CN*: coordination numbers; [b] *R*: bond distance; [c] σ^2: Debye-Waller factors; [d] ΔE_0: the inner potential correction. *R* factor: goodness of fit. S_0^2, 0.847, was obtained from the experimental EXAFS fit of the Co_3O_4 reference, by fixing CN as the known crystallographic value to all of the samples.

In normal Co_3O_4, CN of Co-O in CoO_6 octahedrons and CoO_4 tetrahedrons is 6 and 4, respectively, the ratio of CoO_6 octahedrons and CoO_4 tetrahedrons in Co_3O_4 is 2:1, thus the average coordination number of Co-O should be calculated as 5.33, which complies with the result of Co_3O_4 PNAs/CFC in Table S1.

The CN of Co-O and Co-Co of Co_3O_4 PNAs/CFC are similar to that of standard Co_3O_4 with larger σ^2 value, indicating that Co_3O_4 PNAs/CFC presents typical chemical structure of Co_3O_4 with slightly higher disorder degree.

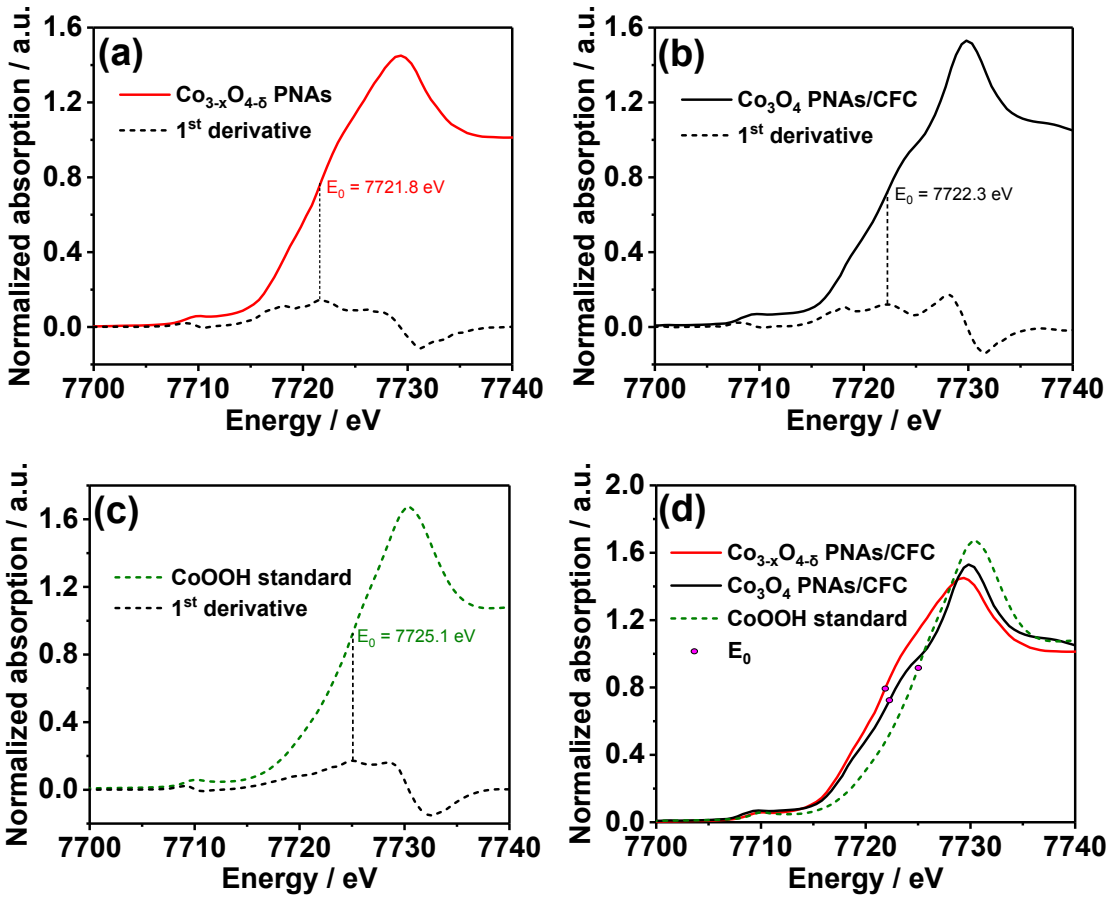

Figure S14 The white line of XANES and the first-order derivative of (a) $Co_{3-x}O_{4-\delta}$ PNAs/CFC, (b) Co_3O_4 PNAs/CFC and (c) CoOOH standard; (d) The white line of XANES and threshold energy (E_0) of $Co_{3-x}O_{4-\delta}$ PNAs/CFC, Co_3O_4 PNAs/CFC and CoOOH standard.

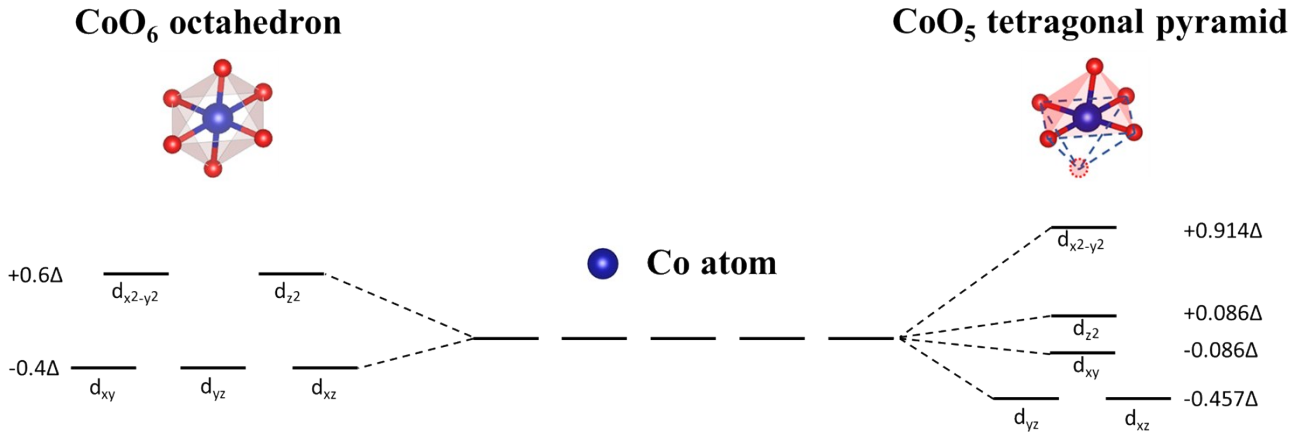

Figure S15 Splitting of 3d orbits of Co atom in octahedral and tetragonal pyramidic coordinative fields.

Table S2. Electrocatalytic activities of various Co_3O_4 OER catalysts.

Electrocatalysts	$\eta_{10\ mA\ cm^{-2}}$ / mV	Tafel slope / mV dec^{-1}	References
$Co_{3-x}O_{4-\delta}$ PNAs/CFC	**291**	**58.12**	**This work**
Co_3O_4/CoO	302	68.6	*Small* 2019, 15, 1904903
Co_3O_4@BP	400	63	*ACS Appl. Mater. Interfaces* 2019, 11, 17459
Se/Ni-Co_3O_4-0.4/CP	290	69.9	*ACS Sustainable Chem. Eng.* 2019, 7, 11901
Co_3O_4@Z67-N700@CeO_2	350	80.7	*J. Mater. Chem. A* 2019, 7, 25853
CoFe LDH/Co_3O_4	290	77	*ChemSusChem* 2019, 12, 4442
Co_3O_4/NC-350	298	69	*Small* 2019, 15, 1904260
Co_3O_{4-x} HoNPs@HPNCS-60	313	37.7	*Angew. Chem. Int. Ed.* 2019, 58, 13840
Co_3O_4/Ag@NrGO	437	-	*Chem. Eur. J.* 2018, 24, 14816
Co_3O_4/Co-Fe oxide DSNBs	297	61	*Adv. Mater.* 2018, 30, 1801211
CoO_x-4h	306	67	*Nano Energy* 2018, 43, 110
Co_3O_4 nanosheets	330	57.8	*ACS Appl. Mater. Interfaces* 2017, 9, 16159
V_O-Co_3O_4	330	67.7	*Energy Environ. Sci.* 2017, 10, 2563
Co_3O_4@CoO SC	430	89	*Nat. Commun.* 2015, 6, 8106
Au/Co_3O_4	370	60	*Adv. Mater.* 2014, 26, 3950
graphene-like holey Co_3O_4 nanosheets	~464	68	*Nano Energy* 2016, 30, 267
Co_3O_4/N-PC	390	72	*Nano Energy* 2015, 12, 1
Reduced Co_3O_4	400	72	*Adv. Energy Mater.* 2014, 4, 1400696
$Co_{3-x}O_4$-500	367	57.2	*ACS Catal.* 2018, 8, 3803
$Co_{3-x}O_4$-700	376	58.9	
BCN-Co_3O_4	394	-	*RSC Adv.* 2016, 6, 79448
Co_3O_4	368	59	*J. Power Sources* 2016, 310, 41
RGO-Co_3O_4	410	85	*J. Mater. Chem. A* 2016, 4, 13534
10%Ni-Co_3O_4	370	83	*ACS Appl. Mater. Interfaces* 2016, 8, 20802
T-3D-Co_3O_4	410	58	*Chemelectrochem.* 2017, 4, 2453
Co_3O_4 sheets	537	134	*Nanoscale.* 2018, 10, 10221
Co_3O_4/NCMT-800	350	-	*J. Mater. Chem. A.* 2017, 5, 20170

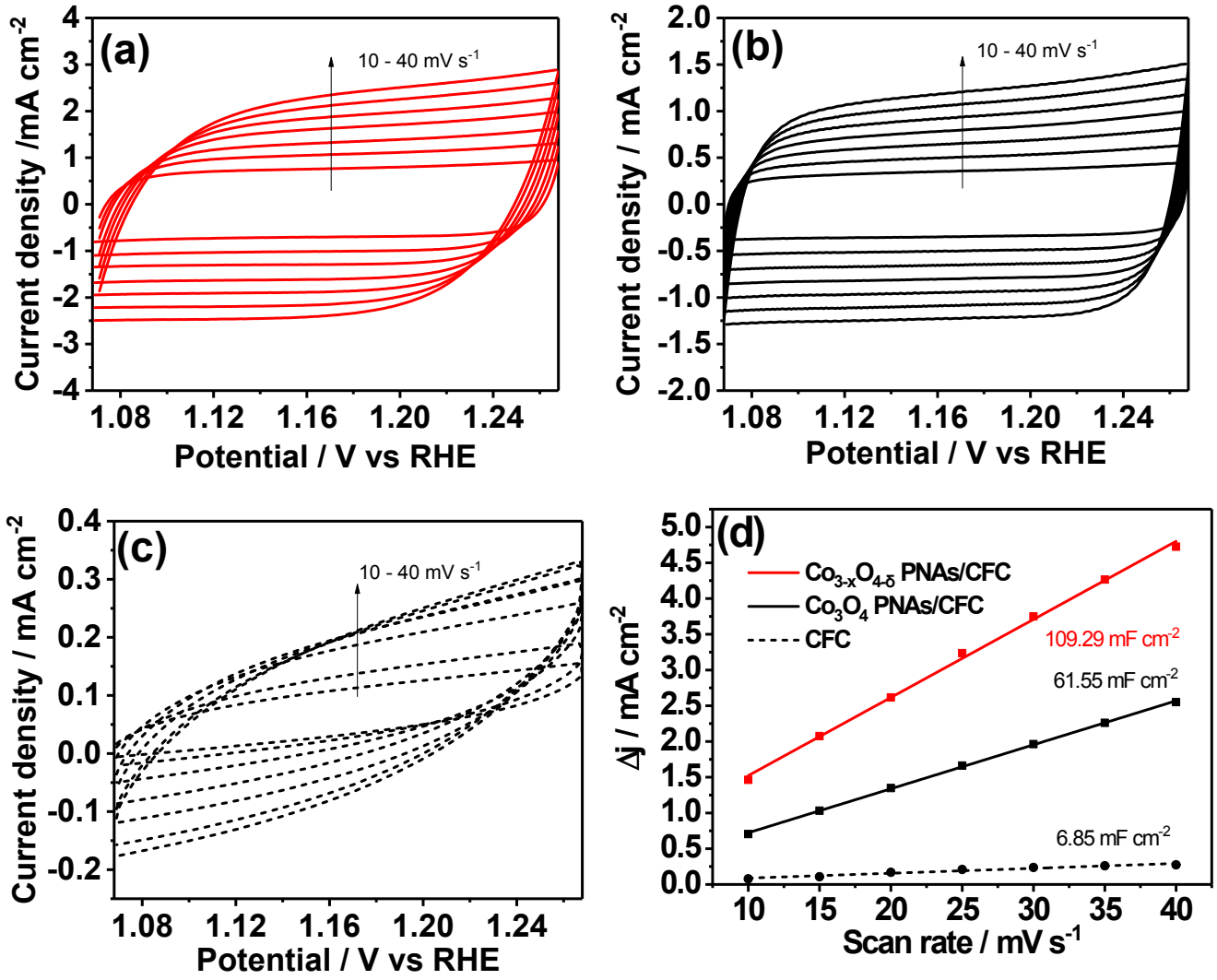

Figure S16 CV curves of (a) $Co_{3-x}O_{4-\delta}$ PNAs/CFC, (b) Co_3O_4 PNAs/CFC and (c) CFC; (d) current density variation plotted against the scan rate, fitted to a linear regression, enables the estimation of the double layer capacitance (C_{dl}).

The electrochemical active areas of $Co_{3-x}O_{4-\delta}$ PNAs/CFC and Co_3O_4 PNAs/CFC was determined by the formula:

$$R_f = \frac{C_{dl}}{60}$$

in which the C_{dl} of samples were deduced by the value of CFC, it was assumed that the C_{dl} of an ideal oxide's unit area is 60 μF cm^{-2}. R_f is the roughness factor.

The electrochemical active area (ECSA) was calculated by the formula:

$$ECSA = R_f \times A$$

where A is the surface area of the electrode. [2]

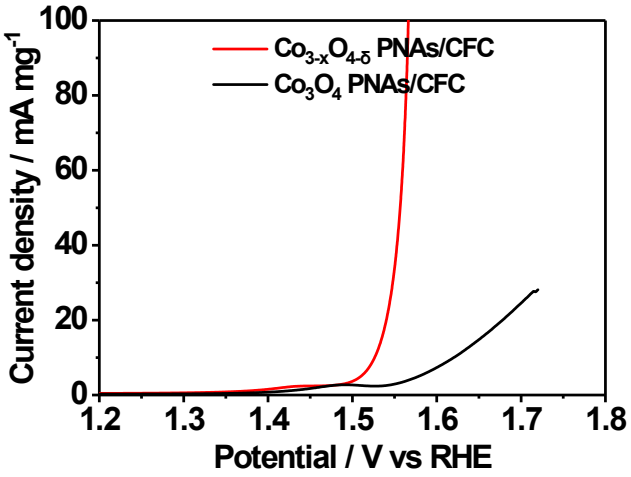

Figure S17 LSV curves of (a) $Co_{3-x}O_{4-\delta}$ PNAs/CFC and (b) Co_3O_4 PNAs/CFC, normalized to the mass of Co_3O_4.

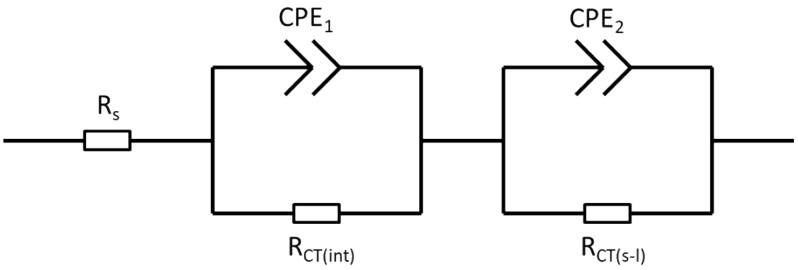

Figure S18 The simplified equivalent circuit model of EIS.

Table S3 The fitting factor of each circuit component of $Co_{3-x}O_{4-\delta}$ PNAs/CFC and Co_3O_4 PNAs/CFC.

sample	$R_{CT(int)}$	$R_{CT(s-l)}$	R_s	CPE_1	CPE_2
$Co_{3-x}O_{4-\delta}$ PNAs/CFC	0.5114	8.023	5.168	0.0005285	0.09841
Co_3O_4 PNAs/CFC	8.679	25.45	6.221	0.0002209	0.04569

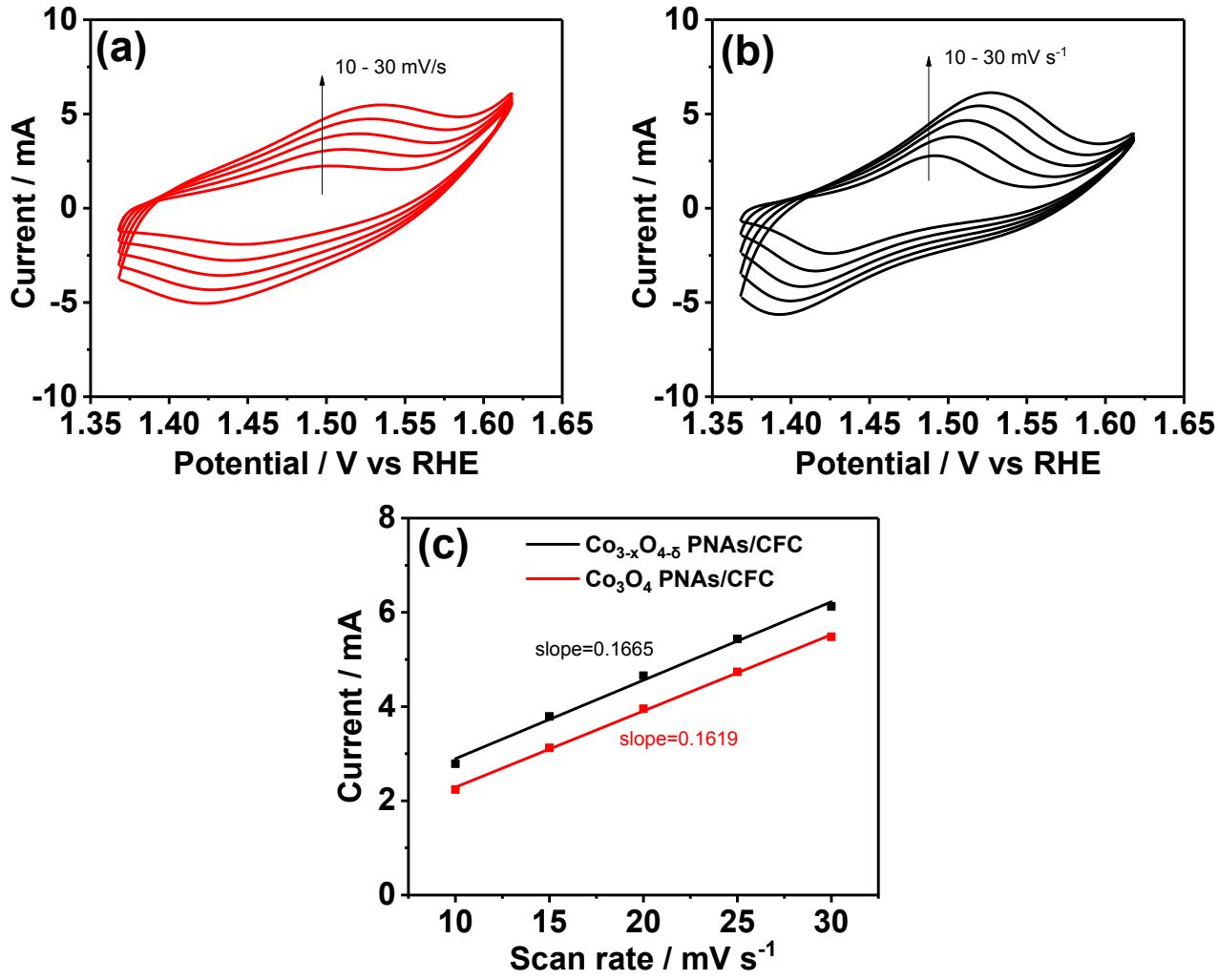

Figure S19 CVs for (a) $Co_{3-x}O_{4-\delta}$ PNAs/CFC and (b) Co_3O_4 PNAs/CFC under different scan rates from10 to 60 mV s^{-1} in 1.0 M KOH; (c) linear relationship of the peak currents vs. scan rates for $Co_{3-x}O_{4-\delta}$ PNAs/CFC and Co_3O_4 PNAs/CFC at different fixed overpotentials.

The number of surface active sites associated with the redox Co species should be first calculated. The linear relationship between the oxidation peak current and the scan rate can be extracted from the electrochemical cyclic voltammetry scans. The slope of the line can be calculated based on the following equation:

$$Slope = \frac{n^2F^2m}{4RT}$$

in which n is the number of electrons transferred in the redox of Co^{3+}/Co^{4+}, F is the Faraday constant, m is the number of active sites (mol), R and T are the ideal gas constant and the absolute temperature, respectively.[3]

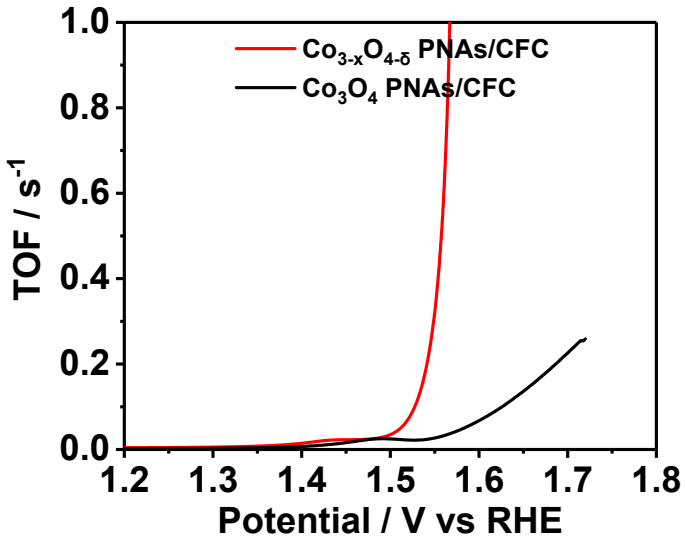

Figure S20 TOF curves of $Co_{3-x}O_{4-\delta}$ PNAs/CFC and Co_3O_4 PNAs/CFC.

The TOF value can be finally calculated using the formula

$$TOF = \frac{JA}{4Fm}$$

in which TOF is based on the number of redox-active sites, J is the current density at a certain overpotential, A is the area of the electrode, 4 indicates the moles of electrons consumed for evolving one mole of O_2 from H_2O, F is the Faraday constant, and m is the number of moles of the active sites.[4]

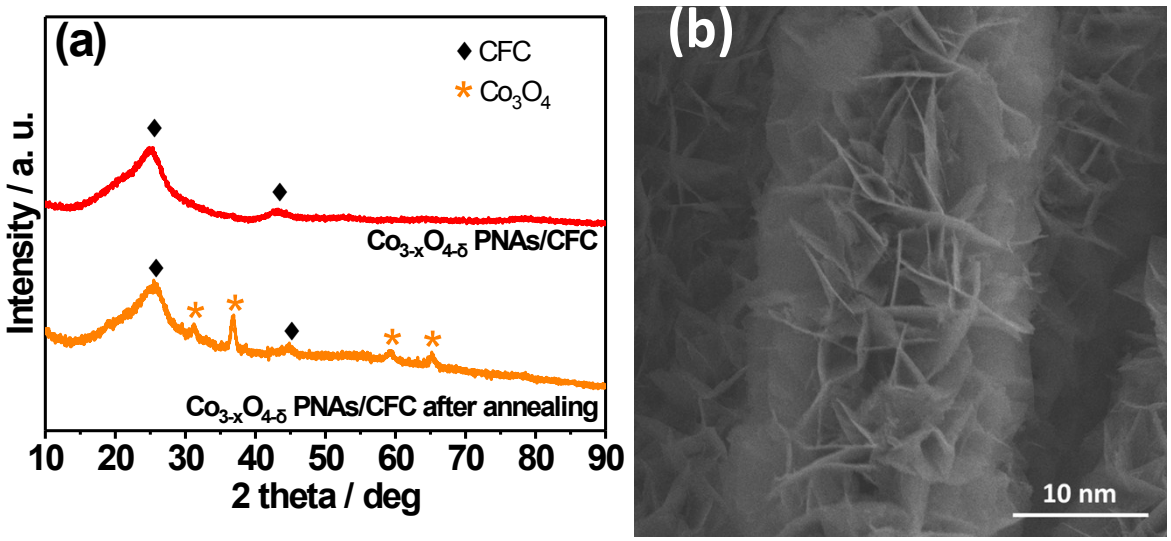

Figure S21 (a) XRD patterns of $Co_{3-x}O_{4-\delta}$ PNAs/CFC and $Co_{3-x}O_{4-\delta}$ PNAs/CFC after annealing; (b) SEM image of $Co_{3-x}O_{4-\delta}$ PNAs/CFC after annealing.

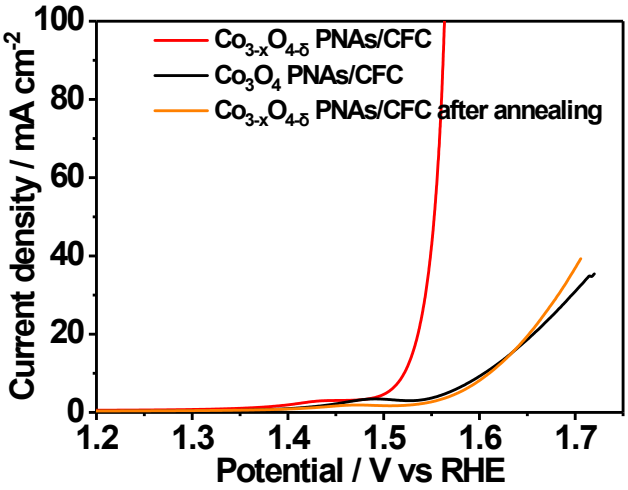

Figure S22 LSV curves of $Co_{3-x}O_{4-\delta}$ PNAs/CFC, Co_3O_4 PNAs/CFC and $Co_{3-x}O_{4-\delta}$ PNAs/CFC after annealing in 1 M KOH at 5 mV s^{-1}.

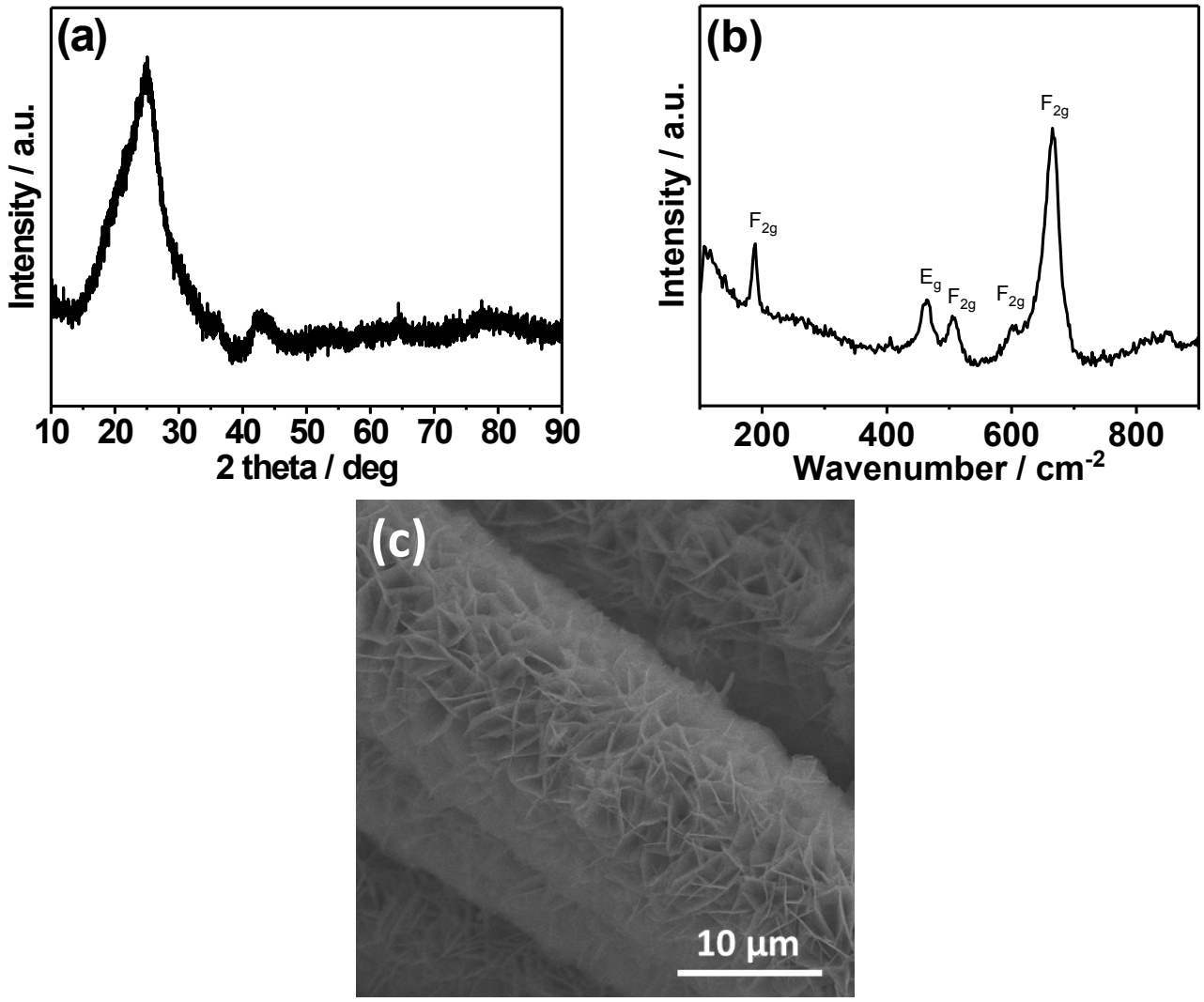

Figure S23 (a) XRD pattern, (b) Raman spectrum, and (c) SEM image of $Co_{3-x}O_{4-\delta}$ PNAs/CFC after the durability test.

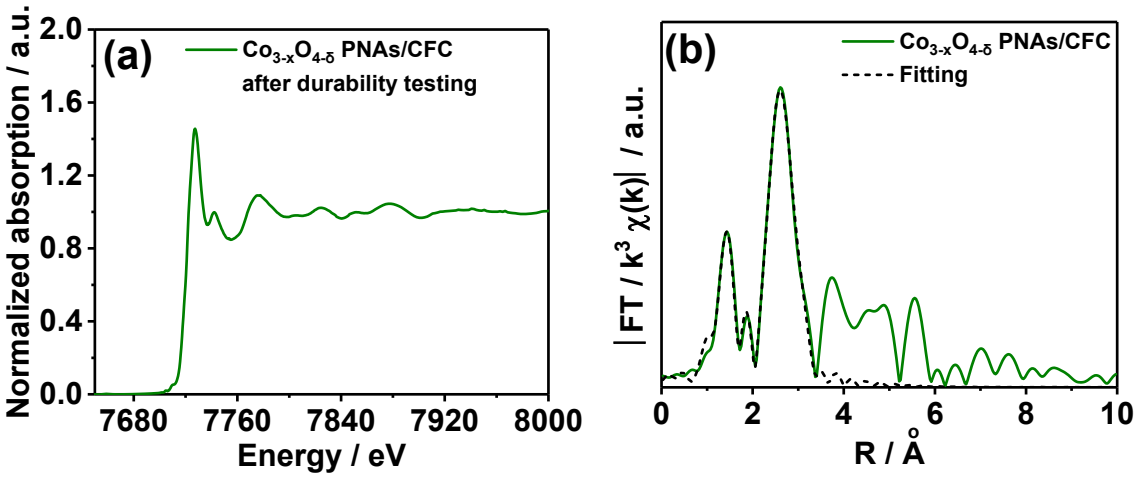

Figure S24 (a) XANES and (b) FT-EXAFS of $Co_{3-x}O_{4-\delta}$ PNAs/CFC after the durability test.

Table S4. EXAFS fitting parameters at the Co K-edge for $Co_{3-x}O_{4-\delta}$ PNAs/CFC after durability test.

Sample	Shell	*CN* [a]	*R* (Å) [b]	σ^2 (Å^2·10^3) [c]	ΔE_0 (eV) [d]	*R*
$Co_{3-x}O_{4-\delta}$ PNAs/CFC after durability test	Co-O	2.5	1.91	3.9	-8.4	
	Co_{Oh}-Co_{Oh}	5.0	2.96	7.9	-6.7	
	Co-Co_{Td}	4.2	3.33	6.6		

[a] *CN*: coordination numbers; [b] *R*: bond distance; [c] σ^2: Debye-Waller factors; [d] ΔE_0: the inner potential correction. *R* factor: goodness of fit. *S*02, 0.847, was obtained from the experimental EXAFS fit of Co_3O_4 reference by fixing CN as the known crystallographic value and was fixed to all the samples.

The EXAFS fitting parameters of $Co_{3-x}O_{4-\delta}$ PNAs/CFC after durability test exhibited slightly change compared to those of $Co_{3-x}O_{4-\delta}$ PNAs/CFC shown in Table S4. The CN of Co-O and Co-Co_{Td} lowered after durability test, which means that long-term OER process at anodic potential may further induced the structural defects of Co tetrahedrons. Conversely, the CN of Co_{Oh}-Co_{Oh} slightly increased from 4.0 to 5.0, this phenomenon may be attributed to the measurement error of CN that is within 20% or little generation of $Co(OH)_2$ in the alkaline aqueous. XRD pattern and Raman spectrum shown in Figure S23 indicate that $Co_{3-x}O_{4-\delta}$ PNAs/CFC remained low crystalline Co_3O_4 phase without obvious impurity after durability test, thus we can conclude that microstructure didn't undergo large variation during the durability test.

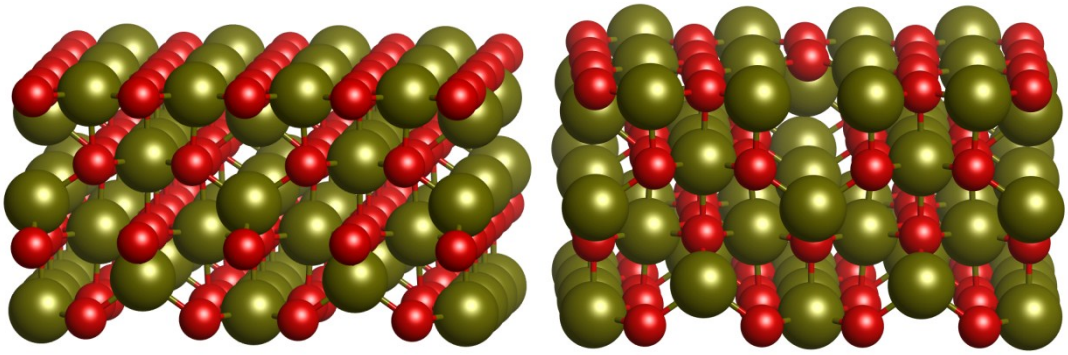

Figure S25 Calculation models of (a) perfect Co_3O_4 and (b) $Co_{3-x}O_{4-\delta}$ with tetrahedral CoO_4 vacancies.

Table S5 Molecular energy used for calculations.

	H_2O	OH^-	O_2	H_2
G (eV)	−14.32259985	−10.90832303	−10.0680924	−6.82855365

The energy of O_2 was calculated by $G(O_2) = G(2H_2O) - 2G(H_2) + 4.92$ eV.
The energy of OH^- was calculated by $G(OH^-) = G(H_2O)\text{-}G(H^+)$.

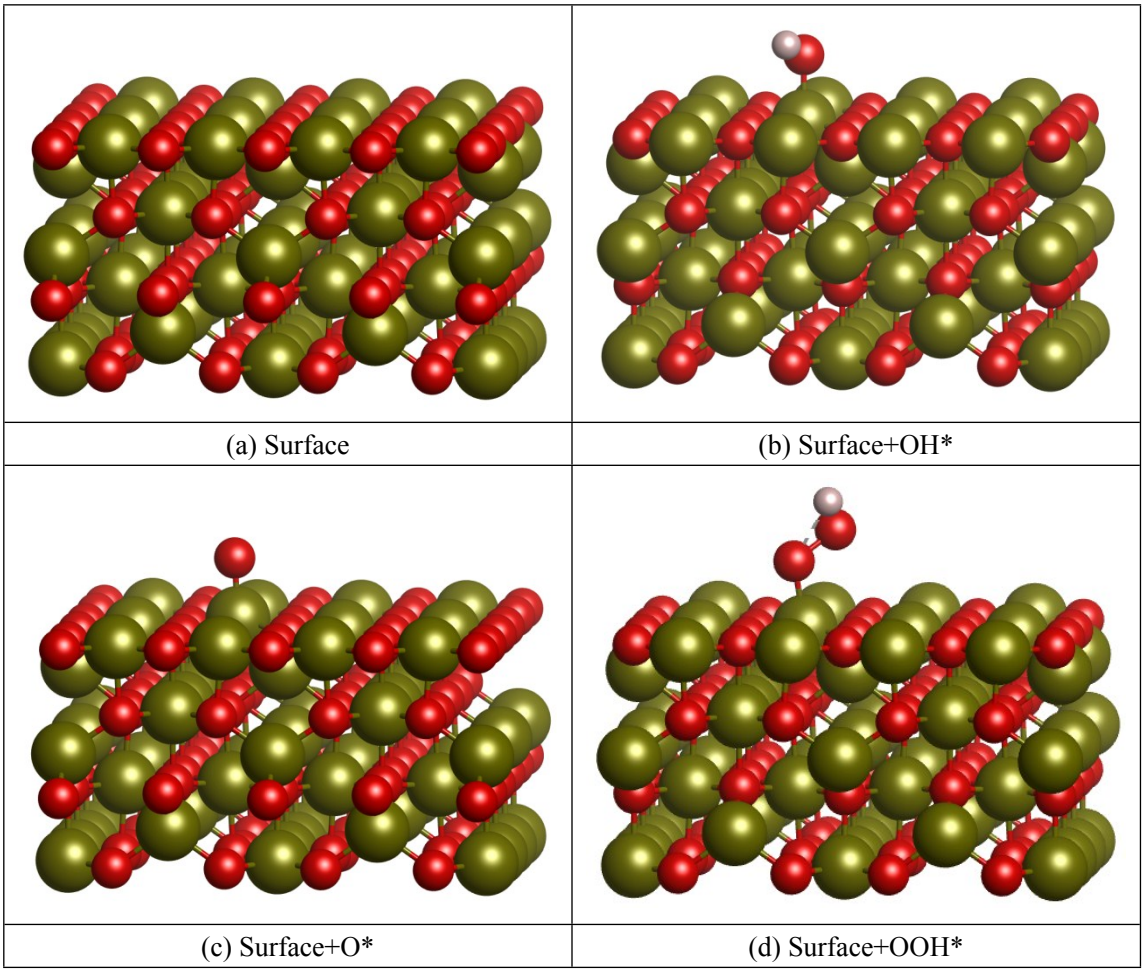

(a) Surface | (b) Surface+OH*

(c) Surface+O* | (d) Surface+OOH*

Figure S26 Optimized configurations of (a) (001) of bare Co_3O_4 and (b) OH*, (c) O*, (d) OOH* species absorbed on (001) of Co_3O_4.

Table S6 Energy of each intermediate species and variation of the Gibbs free energy of each elementary step of Co_3O_4.

	Energy (eV)		
Surface	−714.61808813	ΔG1	0.644141185
Surface+OH	−724.88226997	ΔG2	2.013164385
Surface+O	−719.45482876	ΔG3	1.112610255
Surface+OOH	−729.25054153	ΔG4	1.150084175

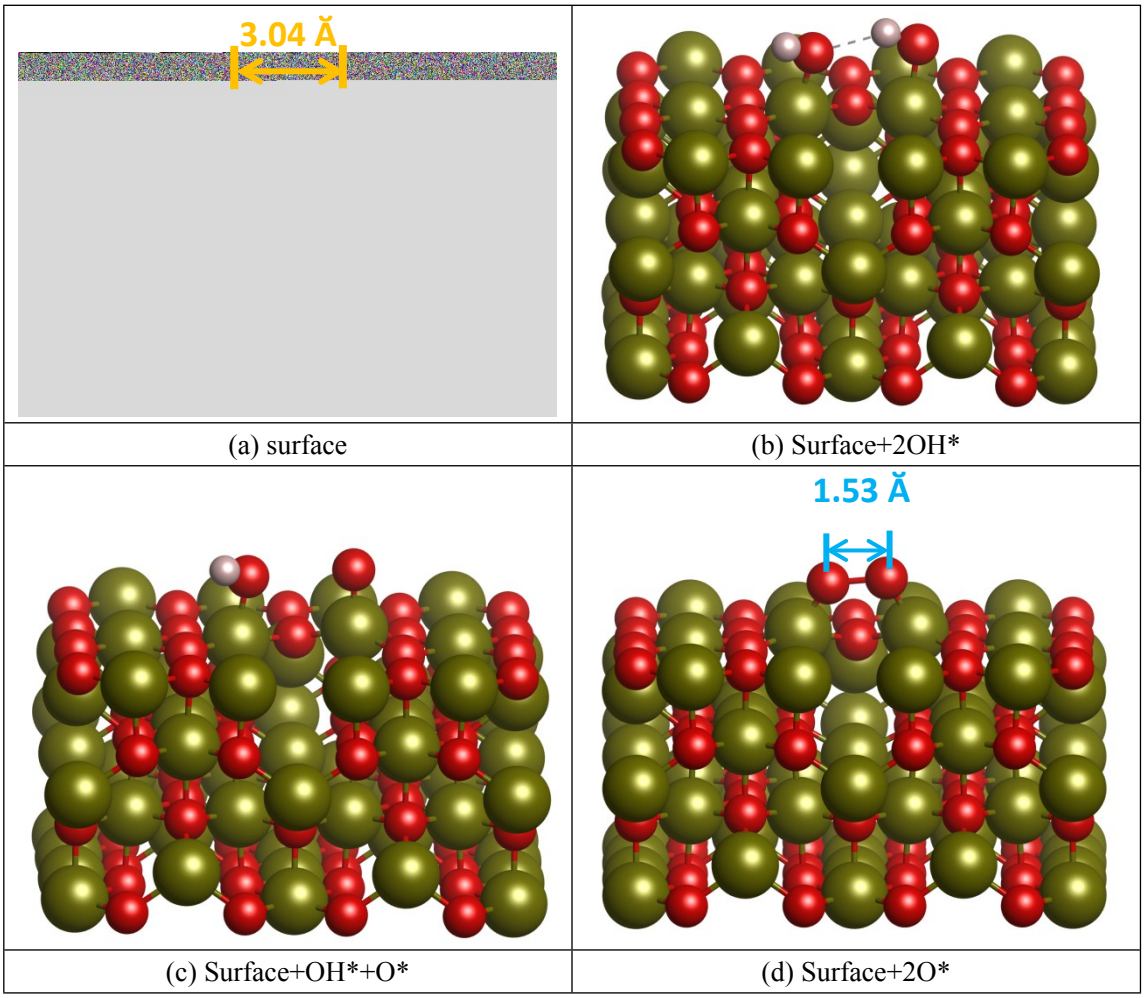

(a) surface (b) Surface+2OH*

(c) Surface+OH*+O* (d) Surface+2O*

Figure S27 Optimized configurations of (a) (001) of bare $Co_{3-x}O_{4-\delta}$ and (b) 2OH*, (c) OH* + O*, and (d) 2O* species absorbed on the oxygen vacancies on (001) of $Co_{3-x}O_{4-\delta}$.

Table S7 Energy of each intermediate species and variation of the Gibbs free energy of each elementary steps of $Co_{3-x}O_{4-\delta}$.

	Energy (eV)		
Surface	−691.98087440	ΔG1	0.51455471
Surface+2OH	−713.28296574	ΔG2	1.911768845
Surface+OH+O	−707.95692007	ΔG3	1.425043005
Surface+2O	−703.11760024	ΔG4	1.06863344

References

[1] S. Meher, G. Rao. *J. Phys. Chem. C* **2011**, *115*, 25543-25556.

[2] R. Zhang, Y. Zhang, L. Pan, G. Shen, N. Mahmood, Y. Ma, Y. Shi, W. Jia, L. Wang, X. Zhang, W. Xu, J. Zou. *ACS Catal.* **2018**, *8*, 3803-3811.

[3] D. Wu, Y. Wei, X. Ren, X. Ji, Y. Liu, X. Guo, Z. Liu, A. Asiri, Q, Wei, X. Sun. *Adv. Mater*. **2018**, *30*, 1705366.